Magnetic field evolution of spin blockade in Ge/Si nanowire double quantum dots

A. Zarassi, Z. Su, J. Danon, J. Schwenderling, M. Hocevar, B. M. Nguyen, J. Yoo, S. A. Dayeh, and S. M. Frolov

Phys. Rev. B **95**, 155416 — Published 12 April 2017

DOI: 10.1103/PhysRevB.95.155416

Magnetic Field Evolution of Spin Blockade in Ge/Si Nanowire Double Quantum Dots

A. Zarassi,[1,*] Z. Su,[1,*] J. Danon,[2] J. Schwenderling,[1,3] M. Hocevar,[4]
B. M. Nguyen,[5] J. Yoo,[5] S. A. Dayeh,[6,7,8] and S. M. Frolov[1,†]

[1]*Department of Physics and Astronomy, University of Pittsburgh, Pittsburgh, PA 15260, USA*
[2]*Department of Physics, NTNU, Norwegian University of Science and Technology, 7491 Trondheim, Norway*
[3]*RWTH Aachen University, 52062 Aachen, Germany*
[4]*Institut Néel, CNRS, F-38000 Grenoble, France*
[5]*Center for Integrated Nanotechnologies, Los Alamos National Laboratory, Los Alamos, NM 87545, USA*
[6]*Department of Electrical and Computer Engineering, University of California, San Diego, La Jolla, CA 92037, USA*
[7]*Graduate Program of Materials Science and Engineering, University of California, San Diego, La Jolla, CA 92037, USA*
[8]*Department of NanoEngineering, University of California, San Diego, La Jolla, CA 92037, USA*

(Dated: February 16, 2017)

We perform transport measurements on double quantum dots defined in Ge/Si core/shell nanowires and focus on Pauli spin blockade in the regime where tens of holes occupy each dot. We identify spin blockade through the magnetic field dependence of the leakage current. We find both a dip and a peak in the leakage current at zero field. We analyze this behavior in terms of quantum dot parameters such as coupling to the leads, interdot tunnel coupling as well as spin-orbit interaction. We estimate a lower bound on the spin-orbit parameter corresponding to an upper bound of $l_{\mathrm{so}} = 500$ nm for the Rashba spin-orbit length. We also extract effective Landé g-factors up to 8.0 from field-dependent spin blockade measurements.

I. INTRODUCTION

Studies of spin blockade in quantum dots are largely motivated by the proposals to build a spin-based quantum computer[1], as spin blockade can be used for qubit initialization and readout[2,3]. At the same time, spin blockade and its lifting mechanisms offer a direct insight into spin relaxation and dephasing processes in semiconductors and provide deeper understanding of interactions between spin localized in a quantum dot and its environment, be it the lattice and its vibrations or nuclear spins, spin-orbit interaction, or coupling to spins in nearby dots or in the lead reservoirs[4–8].

Holes in Ge/Si nanowires offer a relatively unexplored platform for such studies[9]. On the one hand, hyperfine interaction is expected to be greatly reduced owing to the low abundance of nonzero nuclear spin isotopes in the group IV materials[10]. Moreover, holes weakly couple to nuclear spins due to their p-wave Bloch wave symmetry, thus they are expected to come with longer spin relaxation times[11]. Heavy/light hole degeneracy may also influence the spin blockade regime[12]. On the other hand, spin-orbit interaction is predicted[13] and suggested by experiments[14–17] to be strong in Ge/Si core/shell nanowires. This offers a path to electrical spin manipulation [18,19], as well as to realizing Majorana fermions[20–23].

In this work we perform transport measurements on electrostatically defined double quantum dots[2] made in Ge/Si core/shell nanowires, and detect Pauli spin blockade at several charge degeneracy points. We expand and adapt a previously developed rate equation model to analyze the magnetic-field evolution of the leakage current[24]. We also extract relatively large effective g-factors, up to 8.0 [25–27], which is promising for Majorana fermion and spin qubit implementations.

II. EXPERIMENTAL METHODS

The devices are fabricated on n-doped Si substrates covered with 500 nm of thermal silicon oxide and patterned with local gate arrays of Ti/Au stripes with a center to center distance of 60 nm. The gates are covered by a 10 nm layer of HfO_2 dielectric. Using a micromanipulator[28] the nanowires with a typical length of 3–5 μm, core diameter of 20–30 nm, and shell thickness of 2 nm are placed on top of these gates as shown in the inset of Fig. 1. After wet etching with buffered hydrofluoric acid, we sputter 15 nm of Al followed by 42 nm of NbTiN on lithographically defined source and drain electrodes to make ohmic contacts along with the contacts to the gates. We note that despite the fact that Al and NbTiN are both superconductors the contact between the leads and the nanowire has high resistance and low transparency in these devices, therefore no effects of induced superconductivity are observed on the dots as opposed to nominally the same devices that showed high contact transparency[29]. Furthermore, the applied source-drain bias exceeds the superconducting gap of NbTiN, which remains superconducting at all fields applied here. Thus we do not consider any contribution from the superconductivity of the leads on the leakage current. The measurements are performed in a dilution refrigerator at a base temperature of 30 mK.

The double quantum dot is defined by applying positive voltages to three adjacent gates: G1 and G3 are used to set the outer barriers, and G2 defines the interdot barrier. Since all three gates are in close proximity they all

influence the charge occupation of the dots, as well as all three tunneling barriers.

III. EXPERIMENTAL RESULTS

The main panel of Fig. 1 shows the measured double dot charge stability diagram which consists of a grid of charge degeneracy points connected by co-tunneling lines at higher charge occupations. Many charge degeneracy points are observed before the gate-induced energy barriers to the source and drain get too high to detect the current at the positive gate voltage extremes of the plot. This is in strong contrast with quantum dots defined using similar gates in InAs[8] or InSb[30] nanowires, where only a few charge degeneracy points are visible between complete pinch-off and the open transmission regime. The current is too low to measure at the charge degeneracy points corresponding to the last few holes in both dots, meaning that the tunneling barriers pinch off completely before the dots are emptied. In the regime studied here both dots still contain tens of holes. This is confirmed by asymmetric gate tuning such that as holes are expelled from one dot, the occupation of the other dot is increased and the tunneling barrier is lowered to ensure detectable current. The fact that so many holes fit in a small volume of a double dot (less than 120 nm

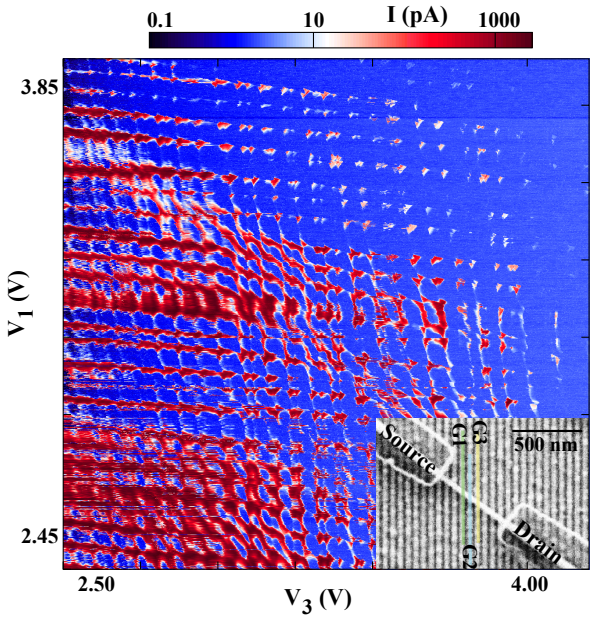

FIG. 1. Current through the double dot as a function of voltage on G1 (V_1) versus voltage on G3 (V_3) at a fixed voltage on G2. The measurement is taken with a source-drain bias of 4 mV and at zero magnetic field. The inset shows a scanning electron micrograph of a representative Ge/Si nanowire device with Al/NbTiN lithographic contacts (labeled "Source" and "Drain") and tuning gate electrodes labeled G1 to G3. The other gates are fixed at zero voltage.

length and 30 nm diameter) is consistent with the large effective hole masses as compared to those of electrons in III-V semiconductors, indicating that the hole wavefunctions are predominantly of a heavy-hole character.

In double quantum dots with multiple charges per dot, spin blockade does not necessarily occur at each (odd, odd) to (even, even) charge transition as expected for simple few-electron quantum dots[2,8,30–33]. In fact, spin blockade may not occur for multiple transitions in a row[34]. This can be either due to the complex spin structure of the higher orbital states or due to a suppressed energy splitting between the ground state singlet and a higher orbital triplet.

When spin blockade does occur we assume that it can be effectively understood in the same way as the simplest $(1,1) \rightarrow (0,2)$ spin blockade: Close to zero detuning, the n'th hole in the source dot can only enter the drain dot if it can form a spin-singlet state with the m'th hole on the drain dot. Entering an $(n-1, m+1)$ state in a triplet configuration requires occupation of a higher orbital state which becomes energetically accessible only when an additionally applied interdot energy level detuning ε exceeds the singlet-triplet energy level splitting in the drain dot. For small detuning the system is thus expected to be blocked in one of the three triplet states, which are in principle degenerate and split in energy under the influence of a magnetic field due to the Zeeman effect. For clarity we will refer to the (n,m) states as $(1,1)$ and to the $(n-1, m+1)$ states as $(0,2)$. Current through the double dot in the spin blockade regime due to various spin non-conserving processes is referred to as the leakage current.

The primary signature of spin blockade in this study comes from the magnetic field dependence of the leakage current (Fig. 2), which can be explained in terms of the simple spin blockade picture described above. We vary the (1,1) to (0,2) energy level detuning, ε by scanning G1 and G3 perpendicular to the base of bias triangles (as indicated in the inset), while stepping the magnetic field. The suppressed current observed for $0 < \varepsilon \lesssim 2$ meV is associated with spin blockade, and we interpret the sudden rise in current at $\varepsilon \approx 2$ meV as the $(0,2)$ triplet states becoming energetically accessible from the $(1,1)$ triplet states, thus lifting the blockade. The associated singlet-triplet splitting of ~ 2 meV is representative of the several charge degeneracy points studied (see supplemental material).

A smaller rise in the leakage current at lower detuning, marked with the tilted dashed line in Fig. 2, is assigned to a resonance between the lowest $(1,1)$ state T_+ and the singlet $S(0,2)$ state: Below this resonance (for smaller ε), $S(0,2)$ is energetically not accessible from the ground state $T_+(1,1)$ and the system is in Coulomb blockade. Since the energy of $S(0,2)$ is not expected to depend on the magnetic field, the B-dependence of this resonance reflects the B-dependence of the energy of $T_+(1,1)$. The pattern formed by two current resonances marked by dashed lines $T_+(1,1) \rightarrow T(0,2)$ and $T_+(1,1) \rightarrow S(0,2)$ is

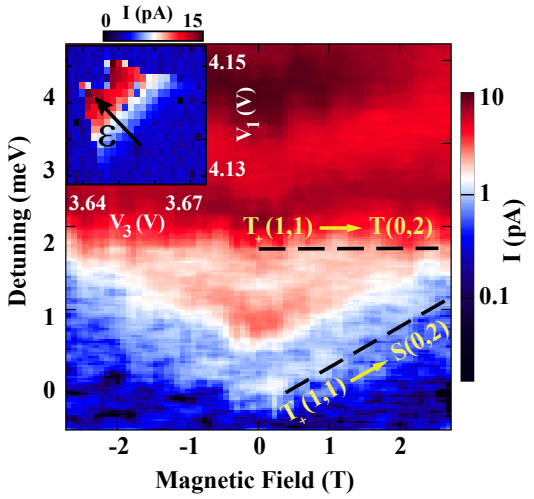

FIG. 2. Current through the double quantum dot measured as a function of the detuning ε and the magnetic field B, with an applied source-drain voltage of $V_{SD} = 6.5$ mV. The magnetic field is applied normal to the substrate plane. The resonances associated with $T_+(1,1) \rightarrow T_+(0,2)$ and $T_+(1,1) \rightarrow S(0,2)$ transitions are marked with dashed lines. From the field dependence of the latter we find $g = 8.0 \pm 0.2$. Inset: the charge degeneracy point at finite bias with the detuning axis used in the main panel indicated by ε.

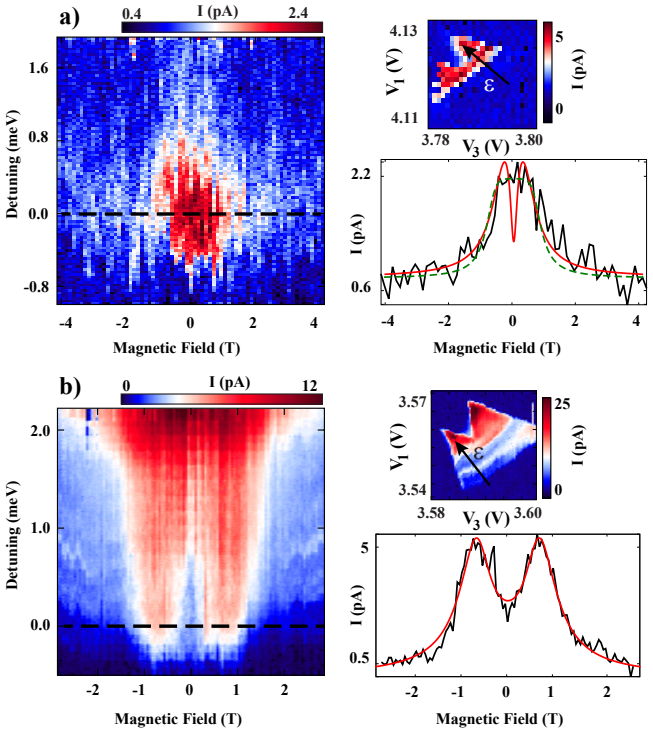

FIG. 3. Magnetic field evolution of the leakage current in two different spin blockaded transport configurations. In both cases the field is applied in the plane of the nanowire and gates, perpendicular to the gates but making an angle of $\sim 30^\circ$ with the wire. In the left panels we show the dependence of the leakage current on magnetic field and detuning, and on the right side we show the corresponding charge degeneracy points (top) and a line cut of the data at zero detuning (bottom). The zero-detuning cuts include fits to the theory presented in the main text. (a) In this configuration, where a bias voltage $V_{SD} = 6.5$ mV is applied, the leakage current has a single-peak structure both as function of the detuning and magnetic field. The corresponding charge stability diagram is taken at $B = 5$ T. In the figure we plot two different theory curves on top of the data, both with $\xi = 0.03$, $g = 4.4$, and an added constant current of 0.8 pA to account for the background signal observed in the data. We further used $\Gamma = 300$ MHz, $t = 50$ μeV, $\gamma = 0.0075$, and $\alpha = 0.4$ (solid red curve) and $\Gamma = 25$ MHz, $t = 150$ μeV, $\gamma = 0.66$, and $\alpha = 0.4$ (dashed green curve). (b) Leakage current at a different charge degeneracy point, with $V_{SD} = 4$ mV. The corresponding bias triangle is taken at $B = 0$ T. Here the current shows a double-peak structure in the magnetic field, which can also be seen in the zero-detuning cut. The theory curve (red solid line) uses $\xi = 0.03$, $g = 4$, $\Gamma = 256$ MHz, $t = 150$ μeV, $\gamma = 0.061$, and $\alpha = 0.37$.

the main signature of spin blockade in this study. Note that a copy resonance follows the $T_+(1,1) \rightarrow S(0,2)$ transition in field, which is not accounted for in the simple spin blockade picture used here.

Using the slope of the resonance labeled $T_+(1,1) \rightarrow S(0,2)$, we obtain $g = 8.0 \pm 0.2$ for Fig. 2. While full g-tensor measurements were not performed, we find lower g-factors for fields deviating from normal to the substrate, in agreement with other studies (see supplemental material)[26,27]. The highest g-factors extracted here are larger than previously reported for Ge/Si nanowires[15,26,27]. One possible reason for this is larger wire diameters used here: indeed, a relevant theory predicts diameter-dependent g-factors[13].

In Fig. 3a,b (left panels) we plot the measured leakage current in the spin blockade regime of two representative charge degeneracy points which show a qualitatively different field-dependent behavior. The current in Fig. 3(a) shows a single peak centered at zero field, whereas in Fig. 3(b) we observe a double-peak structure with a dip at zero magnetic field. We note that beyond the difference in charge numbers, we cannot independently quantify differences in other double dot parameters across the two regimes of Fig. 3. We speculate that the interdot tunnel coupling as well as the couplings to the leads are not the same in the two regimes.

A zero-field dip in the leakage current is known to occur in double dots hosted in materials with strong spin-orbit interaction[6,8,35–37]. The dip is usually explained in terms of a competition between different types of spin-mixing processes: The combination of spin-orbit interaction and Zeeman splitting due to the applied field enables transitions between triplet and singlet configurations. This mechanism becomes more efficient at higher magnetic field and thus it produces a dip in the leakage current around zero field[24]. Other processes that mix spin states, such as the hyperfine interaction between the electrons or holes and the nuclear spins in the host material[38] or

spin-flip cotunneling processes with the leads[39], can be independent of the magnetic field or even become less efficient with increasing B. If one of such processes provides the dominant spin-mixing mechanism, then there will appear no dip in the current around zero field. Since the spin-orbit-mediated mechanism scales with the interdot tunnel coupling, one can expect to observe a transition from having a zero-field dip to no zero-field dip when changing the tuning of the double dot.

IV. THEORETICAL MODEL

Ignoring the potentially more complicated nature of spin blockade in the valence band, we assume that in the present case we can describe the leakage current with a model based on the following ingredients: (i) $S(1,1)$, has the same singlet configuration as $S(0,2)$ and is thus strongly coupled to that state, with a coupling energy t. (ii) The state $S(0,2)$ decays to the drain lead with a rate Γ. Immediately after such a transition a new hole enters the system from the source, bringing it in one of the $(1,1)$ states again. (iii) $T_\pm(1,1)$ split off in energy when a magnetic field is applied. (iv) Spin-orbit interaction results in a coherent non-spin-conserving coupling between the $(1,1)$ triplet states and $S(0,2)$. The energy scale characterizing spin-orbit coupling $t_{\rm so}$ is proportional to t. (v) There can be other spin-mixing and spin-relaxation processes causing transitions between the different $(1,1)$ states.

In our data both the dip and the peak are relatively wide: they appear on a field scale of $B \sim 1$ T which is of the order of 3 K. First of all, this rules out hyperfine interaction as the dominant spin-mixing mechanism in the single-peak data of Fig. 3a. Hyperfine interaction is known to lift spin blockade around zero field producing a peak in current, but the width of the hyperfine peak is comparable to the typical magnitude of the effective nuclear fields in the dots. We estimate the effective nuclear fields in the present system to be less than 10 mT, which is orders of magnitude smaller than the peak width observed here[40]. Secondly, the analytic theory of Ref. 24, which is often used to extract model parameters such as the magnitude of spin-relaxation rates and $\alpha = t_{\rm so}/t$, is valid for $t, t_{\rm so}, B \ll \Gamma$ and also assumes the spin-relaxation rates to be isotropic, based on the assumption $B \ll T$, where T is the temperature. From here on we will use $\hbar = k_{\rm B} = g\mu_{\rm B} = e = 1$. In the present case, however, we have $B \gg T$ for most fields of interest, and spin relaxation will thus mostly be directed towards the $(1,1)$ ground state instead. Furthermore, the suppression of current at the highest fields could indicate that B exceeds at these fields the effective level width of $S(0,2)$ by such an amount that the system is pushed into a Coulomb blockade in the lowest-lying $(1,1)$ triplet state.

We thus cannot straightforwardly apply the theory of Ref. 24 to model the data shown in Fig. 3. Instead we present a modified version of the theory, where we include only spin relaxation to the ground state and do not expand in large Γ. We start from the five-level Hamiltonian

$$H = \begin{pmatrix} 0 & iB & 0 & 0 & i\alpha t \\ -iB & 0 & 0 & 0 & i\alpha t \\ 0 & 0 & 0 & 0 & i\alpha t \\ 0 & 0 & 0 & 0 & t \\ -i\alpha t & -i\alpha t & -i\alpha t & t & 0 \end{pmatrix}, \qquad (1)$$

written in the basis $\{|T_x\rangle, |T_y\rangle, |T_z\rangle, |S\rangle, |S_{02}\rangle\}$, where $|T_{x,y}\rangle = i^{1/2\mp 1/2}\{|T_-\rangle \mp |T_+\rangle\}/\sqrt{2}$ and $|T_z\rangle = |T_0\rangle$ are the three $(1,1)$ triplet levels and $|S\rangle$ and $|S_{02}\rangle$ the $(1,1)$ and $(0,2)$ singlets, respectively. The interdot detuning was set to zero and α parametrizes the strength of the effective spin-orbit interaction in the dots, where $\alpha \sim 1$ corresponds to the strong limit. In principle, the three α's coupling $|T_{x,y,z}\rangle$ to $|S_{02}\rangle$ can be different, constituting a vector $\boldsymbol{\alpha} = (\alpha_x, \alpha_y, \alpha_z)$ (see Ref. 24). The length of this vector corresponds to the strength of the spin-orbit interaction and its direction is related to the direction of the effective spin-orbit field. In a physical nanowire, the precise orientation of $\boldsymbol{\alpha}$ depends on many details and is hard to predict. We therefore make the simplifying assumption that all three components are of the same magnitude. We diagonalize the Hamiltonian and use its eigenbasis to write a time-evolution equation for the density matrix[24],

$$\frac{d\hat{\rho}}{dt} = -i[H^{\rm diag}, \hat{\rho}] + \boldsymbol{\Gamma}\hat{\rho} + \boldsymbol{\Gamma}_{\rm rel}\hat{\rho}. \qquad (2)$$

The operator $\boldsymbol{\Gamma}$ describes (i) decay of all states $|n\rangle$ (with $n = 0 \ldots 4$) to the drain lead with the rates $\Gamma|\langle n|S_{02}\rangle|^2$ and (ii) immediate reload into one of the eigenstates with the probabilities $\{1 - |\langle n|S_{02}\rangle|^2\}/4$. For the relaxation operator $\boldsymbol{\Gamma}_{\rm rel}$ we take a simple form: We assume that all four excited states relax with the same rate $\Gamma_{\rm rel}$ to the ground state. At $B = 0$ this ground state is an equal superposition of $|S_{02}\rangle$ and the optimally coupled $(1,1)$ state $|m\rangle = \{|S\rangle - i\alpha\mathbb{1}\cdot|\vec{T}\rangle\}/\sqrt{1+3\alpha^2}$, and for $B \to \infty$ it develops into a pure $|T_+\rangle$-state.

We first discuss this model on a qualitative level, and investigate how it differs from the model of Ref. 24. For small fields, $B \ll \Gamma$, the different spin relaxation model used here only yields different numerical factors in some of the results. At $B = 0$ we have three blocked states at zero energy that can relax to the hybridized $(1,1)$–$(0,2)$ ground state which quickly decays to the drain lead; this results on average in four holes being transported through the system in a time $3\Gamma_{\rm rel}^{-1}$, thus yielding a leakage current of $I(0) = \frac{4}{3}\Gamma_{\rm rel}$. Adding a finite magnetic field induces a coupling of $\sim \alpha B$ between two of the blocked states and $|m\rangle$, which provides an alternative escape route and leads to an increase of the current.

This increase becomes significant only when the rate of this escape $\sim (\alpha B)^2\Gamma/t^2$ becomes comparable to $\Gamma_{\rm rel}$, which happens at $B \sim (t/\alpha)\sqrt{\Gamma_{\rm rel}/\Gamma}$. For larger fields the current tends to its maximum value $I_{\rm max} = 4\Gamma_{\rm rel}$,

reached when only one truly blocked state is left and on average four holes are transported in a time $\Gamma_{\rm rel}^{-1}$. We see that this picture predicts a zero-field dip in the current of width $B_{\rm dip} \sim (t/\alpha)\sqrt{\Gamma_{\rm rel}/\Gamma}$ and a maximal suppression of the current, by a factor 3, at $B = 0$. This is, apart from numerical factors, the same result as found in Ref. 24.

Qualitative differences appear when we investigate what happens at even higher fields. Since Γ is finite in the present model and all relaxation is directed toward the ground state, we can enter a situation of Coulomb blockade in the $(1, 1)$ ground state $|T_+\rangle$. When we increase B, the current will thus eventually be suppressed to zero, producing in general a double-peak structure in $I(B)$. A naïve guess for the field scale where this suppression sets in would be $\sim \Gamma$: The level width of $|S_{02}\rangle$ is set by Γ, and for $B \gtrsim \Gamma$ the escape rate from $|T_+\rangle$ drops gradually to zero. However, the actual field scale of current decay is rather set by the competition of this escape rate with $\Gamma_{\rm rel}$: Only when the B-induced suppression becomes so strong that escape from $|T_+\rangle$ is the main bottleneck for the leakage current, the decrease in current becomes significant. We thus compare this escape rate $\sim (\alpha t)^2\Gamma/B^2$ with $\Gamma_{\rm rel}$ and find an estimate for the width of the overall double-peak structure $B_c \sim \alpha t\sqrt{\Gamma/\Gamma_{\rm rel}}$.

We can also understand how our model could result in an apparent single-peak $I(B)$. Indeed, $B_{\rm dip}$ and B_c show a different dependence on the model parameters, and their ratio $B_{\rm dip}/B_c \sim \Gamma_{\rm rel}/\alpha^2\Gamma$ (which determines the relative visibility of the zero-field dip) could be large or small, depending on the detailed tuning of all parameters. For $B_{\rm dip}/B_c \ll 1$ one could be in the situation where the central dip around zero field is too narrow to be observed.

We will now support these arguments with a more quantitative investigation of the model. We can solve Eq. 2 in steady state, $d\hat{\rho}/dt = 0$, and find the current from the resulting equilibrium occupation probabilities $p_n = \hat{\rho}_{nn}$ as $I = \sum_n p_n\Gamma|\langle n|S_{02}\rangle|^2$, yielding

$$I(B) = \Gamma_{\rm rel}\frac{[w - B^2 + \tau^2][w(1 + 4\gamma) + B^2 - \tau^2]}{6\gamma w^2 + 2B^2\alpha^2t^2}, \quad (3)$$

where we use the notation $w = \sqrt{(B^2 - \tau^2)^2 + 8B^2\alpha^2t^2}$, the small parameter $\gamma = \Gamma_{\rm rel}/\Gamma$, and $\tau = t\sqrt{1 + 3\alpha^2}$ (which is the total tunnel coupling energy). To obtain Eq. 3 we assumed $\gamma \ll 1$, which we will also do below.

The current given by Eq. 3 indeed shows in general a double-peak structure. At zero field we find $I(0) = \frac{4}{3}\Gamma_{\rm rel}$, and the current has two maxima at $B = \pm\tau$ where $I = 4\Gamma_{\rm rel}$. The half-width of the resulting zero-field dip follows as $B_{\rm dip} = t(\sqrt{\beta^2 + 2} - \beta)/\sqrt{2}$, where $\beta = \alpha/\sqrt{6\gamma}$. In the limit of large β (small $\sqrt{\gamma}/\alpha$) we find $B_{\rm dip} \approx t\sqrt{3\gamma}/\alpha$. At high fields, the current drops to zero, and from Eq. 3 we find the half-width-half-maximum of the full double-peak structure to be $B_{\rm c} = t(\sqrt{\beta^2 + 2} + \beta)/\sqrt{2}$ which reduces to $B_c \approx \alpha t/\sqrt{3\gamma}$ for large β. We see that in the limit of small γ these results agree with the conclusions of our qualitative discussion above.

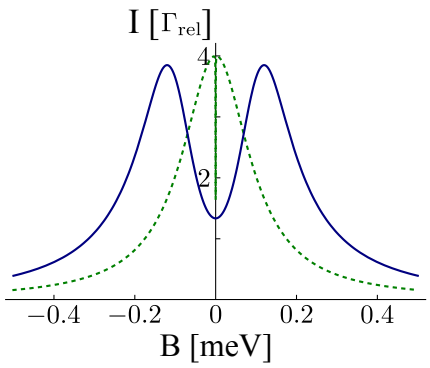

FIG. 4. The current resulting from Eq. 3 for two different sets of parameters: $t = 120$ μeV, $\alpha = 0.1$, and $\gamma = 2 \times 10^{-3}$ (solid blue curve) and $t = 3.5$ μeV, $\alpha = 0.5$, and $\gamma = 10^{-4}$ (dashed green curve).

In Fig. 4 we plot $I(B)$ for two different sets of parameters, illustrating how the model can produce curves that appear to have double-peak as well as single-peak structures. The solid curve shows a clear double-peak structure, which is indeed expected since the "visibility parameter" $B_{\rm dip}/B_c \approx 0.30$ predicts a clearly distinguishable zero-field dip. In contrast, for the dashed curve $B_{\rm dip}/B_c \approx 0.001$. In this case, the current still has a dip around zero field; its width, however, is ~ 1000 times smaller than the overall width of the structure and therefore invisible in the plot. Depending on all other parameters, this situation could thus correspond to an experiment where the leakage current appears to have a single-peak structure.

In order to connect our model to the experimental data in Fig. 3 and facilitate fitting of the model parameters (see below), we include the likely scenario that g-factors in the two dots are different. The effective g-factor for a localized hole depends on many microscopic characteristics, among which the details of the confining potential[13], and is thus expected to differ from dot to dot. Recent studies on similar materials found g-factors differing by 2–5% between two dots in a double dot[37,41]. Such differences are smaller than the error bars in our g-factor measurement, thus they cannot be verified in our devices but they need to be conisdered due to their strong influence on the leakage current. The effect of having different g-factors on the left and right dots (g_L and g_R) is a coherent mixing of $|T_z\rangle$ and $|S\rangle$. As a result, the single blocked state left at finite field $\{|T_z\rangle + i\alpha|S\rangle\}/\sqrt{1 + \alpha^2}$ couples to the decaying state $\{|S\rangle - i\alpha|T_z\rangle\}/\sqrt{1 + \alpha^2}$, thus lifting the blockade. The rate of this decay of the last blocked state is $\Gamma_\xi \sim (\xi B)^2\Gamma/t^2$, where $\xi = \frac{1}{2}(g_L - g_R)/(g_L + g_R)$. This decay competes with $\Gamma_{\rm rel}$ for being the bottleneck for the leakage current: If $\Gamma_\xi \gtrsim \Gamma_{\rm rel}$ then the overall scale of the current will be set by Γ_ξ.

To include the effect of a finite g-factor gradient into our model, we add a term $H_\xi = \xi B\{|T_z\rangle\langle S| + |S\rangle\langle T_z|\}$ to the Hamiltonian (1). We can again solve Eq. 2 in steady

state $d\hat{\rho}/dt = 0$ and arrive at an analytic expression for the current $I(B)$ which we can fit to the data (at this point we do not assume $\gamma \ll 1$). Fixing $\xi = 0.03$, we can obtain reasonable fits to the double-peak data of Fig. 3b (See the supplemental material for an explicit expression for $I(B)$ including a finite ξ). Based on these results, we conclude that spin-orbit parameter α is in the range $\sim$ 0.1–0.4. The single-peak data of Fig. 3a are harder to fit due to lack of features, thus we cannot reasonably narrow down all the fit parameters. However, theory curves with α in the same range as for the double-peak regime can show reasonable agreement, see Fig. 3b.

V. CONCLUSIONS

To conclude, assuming linear Rashba spin-orbit interaction as the dominant relaxation term[13] in these gate-defined double quantum dots with $\alpha = 0.1$–0.4, and a dot-to-dot distance of order 50 nm, we find a spin-orbit length of $l_{\rm so} = 100$–500 nm. While this corresponds to a substantial spin-orbit interaction, it does not greatly exceed that measured in InAs or InSb nanowires. One possibility for this could be that α is not maximal for the field orientation at which data is obtained here as a consequence of spin-orbit anisotropy[30], although the magnetic field was not oriented in the direction expected for the spin-orbit field. Another factor for lower-than-expected spin-orbit interaction is the low strain between the thin Si shell and relatively thick Ge core. Thus, it is conceivable that spin-orbit interaction can be enhanced by tailoring the nanowire morphology. A more detailed insight into spin-orbit coupling and other double dot parameters could be obtained from electric dipole spin resonance.

The Ge/Si nanowire growth was performed at the Center for Integrated Nanotechnologies (CINT), U.S. Department of Energy, Office of Basic Energy Sciences User Facility at Los Alamos National Laboratory (Contract DE-AC52-06NA25396) and Sandia National Laboratories (Contract DE-AC04-94AL85000). We thank T. Baron, R. Chen, S. De Franceschi, P. Gentile, D. Kotekar-Patil, E. Lee and P. Torresani for technical help and useful discussions. S.A.D. acknowledges NSF support under DMR-1503595 and ECCS-1351980. S.M.F. acknowledges NSF DMR-125296, ONR N00014-16-1-2270 and Nanoscience Foundation, Grenoble.

* These authors contributed equally to this work.
† To whom correspondence should be addressed. Email: frolovsm@pitt.edu

[1] D.P. DiVincenzo and D. Loss. Quantum information is physical. *Superlattices and Microstructures*, 23(3):419 – 432, (1998).
[2] R. Hanson, L.P. Kouwenhoven, J.R. Petta, S. Tarucha, and L.M.K. Vandersypen. Spins in few-electron quantum dots. *Rev. Mod. Phys.*, 79:1217–1265, (2007).
[3] J.R. Petta, A.C. Johnson, J.M. Taylor, E.A. Laird, A. Yacoby, M.D. Lukin, C.M. Marcus, M.P. Hanson, and A.C. Gossard. Coherent manipulation of coupled electron spins in semiconductor quantum dots. *Science*, 309(5744):2180–2184, (2005).
[4] F.H.L. Koppens, J.A. Folk, J.M. Elzerman, R. Hanson, L.H. Willems van Beveren, I.T. Vink, H.P. Tranitz, W. Wegscheider, L.P. Kouwenhoven, and L.M.K. Vandersypen. Control and detection of singlet-triplet mixing in a random nuclear field. *Science*, 309(5739):1346–1350, (2005).
[5] A.C. Johnson, J.R. Petta, J.M. Taylor, A. Yacoby, M.D. Lukin, C.M. Marcus, M.P. Hanson, and A.C. Gossard. Triplet-singlet spin relaxation via nuclei in a double quantum dot. *Nature*, 435:925 – 928, (2005).
[6] A. Pfund, I. Shorubalko, K. Ensslin, and R. Leturcq. Suppression of spin relaxation in an inas nanowire double quantum dot. *Phys. Rev. Lett.*, 99:036801, (2007).
[7] A. Pfund, I. Shorubalko, K. Ensslin, and R. Leturcq. Spin-state mixing in inas double quantum dots. *Phys. Rev. B*, 76:161308, (2007).
[8] S. Nadj-Perge, S.M. Frolov, J.W.W. van Tilburg, J. Danon, Yu.V. Nazarov, R. Algra, E.P.A.M. Bakkers, and L.P. Kouwenhoven. Disentangling the effects of spin-orbit and hyperfine interactions on spin blockade. *Phys. Rev. B*, 81:201305, (2010).
[9] W. Lu, J. Xiang, B.P. Timko, Y. Wu, and C.M. Lieber. One-dimensional hole gas in germanium/silicon nanowire heterostructures. *Proc. Natl Acad. Sci. USA*, 102(29):10046–10051, (2005).
[10] Y. Hu, H.O.H. Churchill, D.J. Reilly, J. Xiang, C.M. Lieber, and C.M. Marcus. A ge/si heterostructure nanowire-based double quantum dot with integrated charge sensor. *Nature Nanotech.*, 2:622 – 625, (2005).
[11] J. Fischer, W.A. Coish, D.V. Bulaev, and D. Loss. Spin decoherence of a heavy hole coupled to nuclear spins in a quantum dot. *Phys. Rev. B*, 78:155329, (2008).
[12] F. Pei, E.A. Laird, G.A. Steele, and L.P. Kouwenhoven. Valley-spin blockade and spin resonance in carbon nanotubes. *Nature Nanotech.*, 7:630 – 634, (2012).
[13] C. Kloeffel, M. Trif, and D. Loss. Strong spin-orbit interaction and helical hole states in ge/si nanowires. *Phys. Rev. B*, 84:195314, (2011).
[14] X.J. Hao, T. Tu, G. Cao, C. Zhoe, H.O. Li, G.C. Guo, W.Y. Fung, Z. Ji, G.P. Guo, and W. Lu. Strong and tunable spin-orbit coupling of one-dimentional holes in ge/si core/shell nanowires. *Nano Lett.*, 10:2956 – 2960, (2010).
[15] Y. Hu, F. Kuemmeth, C.M. Lieber, and C.M. Marcus. Hole spin relaxation in ge-si core-shell nanowire qubits. *Nature Nanotech.*, 7:47 – 50, (2012).
[16] A.P. Higginbotham, T.W. Larsen, J. Yao, H. Yan, C.M. Lieber, C.M. Marcus, and F. Kuemmeth. Hole spin coherence in a ge/si heterostructure nanowire. *Nano Lett.*, 14:3582 – 3586, (2014).
[17] A.P. Higginbotham, F. Kuemmeth, T.W. Larsen, M. Fitzpatrick, J. Yao, H. Yan, C.M. Lieber, and C.M. Marcus. Antilocalization of coulomb blockade in a ge/si nanowire. *Phys. Rev. Lett.*, 112:216806, (2014).
[18] K.C. Nowack, F.H.L. Koppens, Yu.V. Nazarov, and

L.M.K. Vandersypen. Coherent control of a single electron spin with electric fields. *Science*, 318(5855):1430–1433, (2007).

[19] S. Nadj-Perge, S.M. Frolov, E.P.A.M. Bakkers, and L.P. Kouwenhoven. Spin-orbit qubit in a semiconductor nanowire. *Nature*, 468:1084 – 1087, (2010).

[20] R.M. Lutchyn, J.D. Sau, and S. Das Sarma. Majorana fermions and a topological phase transition in semiconductor-superconductor heterostructures. *Phys. Rev. Lett.*, 105:077001, (2010).

[21] Y. Oreg, G. Refael, and F. von Oppen. Helical liquids and majorana bound states in quantum wires. *Phys. Rev. Lett.*, 105:177002, (2010).

[22] V. Mourik, K. Zuo, S.M. Frolov, S.R. Plissard, E.P.A.M. Bakkers, and L.P. Kouwenhoven. Signatures of majorana fermions in hybrid superconductor-semiconductor nanowire devices. *Science*, 336(6084):1003–1007, (2012).

[23] F. Maier, J. Klinovaja, and D. Loss. Majorana fermions in ge/si hole nanowires. *Phys. Rev. B*, 90:195421, (2014).

[24] J. Danon and Yu.V. Nazarov. Pauli spin blockade in the presence of strong spin-orbit coupling. *Phys. Rev. B*, 80:041301, (2009).

[25] F. Maier, C. Kloeffel, and D. Loss. Tunable g factor and phonon-mediated hole spin relaxation in ge/si nanowire quantum dots. *Phys. Rev. B*, 87:161305, (2013).

[26] S. Roddaro, A. Fuhrer, P. Brusheim, C. Fasth, H.Q. Xu, L. Samuelson, J. Xiang, and C.M. Lieber. Spin states of holes in Ge/Si nanowire quantum dots. *Phys. Rev. Lett.*, 101:186802, (2008).

[27] M. Brauns, J. Ridderbos, A. Li, E.P.A.M. Bakkers, and F.A. Zwanenburg. Electric-field dependent g-factor anisotropy in ge-si core-shell nanowire quantum dots. *Phys. Rev. B*, 93:121408, (2016).

[28] K. Flöhr, M. Liebmann, K. Sladek, H.Y. Günel, R. Frielinghaus, F. Haas, C. Meyer, H. Hardtdegen, T. Schäpers, D. Grützmacher, and M. Morgenstern. Manipulating inas nanowires with submicrometer precision. *Review of Scientific Instruments*, 82(11), (2011).

[29] Z. Su, A. Zarassi, B.M. Nguyen, J. Yoo, S.A. Dayeh, and S.M. Frolov. High critical magnetic field superconducting contacts to Ge/Si core/shell nanowires. *ArXiv e-prints:1610.03010*, (2016).

[30] S. Nadj-Perge, V.S. Pribiag, J.W.G. van den Berg, K. Zuo, S.R. Plissard, E.P.A.M. Bakkers, S.M. Frolov, and L.P. Kouwenhoven. Spectroscopy of spin-orbit quantum bits in indium antimonide nanowires. *Phys. Rev. Lett.*, 108:166801, (2012).

[31] A. C. Johnson, J. R. Petta, C. M. Marcus, M. P. Hanson, and A. C. Gossard. Singlet-triplet spin blockade and charge sensing in a few-electron double quantum dot. *Phys. Rev. B*, 72:165308, Oct (2005).

[32] H. W. Liu, T. Fujisawa, Y. Ono, H. Inokawa, A. Fujiwara, K. Takashina, and Y. Hirayama. Pauli-spin-blockade transport through a silicon double quantum dot. *Phys. Rev. B*, 77:073310, Feb (2008).

[33] N. Shaji, C. B. Simmons, M. Thalakulam, L. J. Klein, H. Qin, H. Luo, D. E. Savage, M. G. Lagally, A. J. Rimberg, R. Joynt, M. Friesen, R. H. Blick, S. N. Coppersmith, and M. A. Eriksson. Spin blockade and lifetime-enhanced transport in a few-electron si/sige double quantum dot. *Nat Phys*, 4:540 – 544, (2008).

[34] H. O. H. Churchill, A. J. Bestwick, J. W. Harlow, F. Kuemmeth, D. Marcos, C. H. Stwertka, S. K. Watson, and C. M. Marcus. Electron-nuclear interaction in 13c nanotube double quantum dots. *Nat Phys*, 5:321 – 326, (2009).

[35] G. Yamahata, T. Kodera, H.O.H. Churchill, K. Uchida, C.M. Marcus, and S. Oda. Magnetic field dependence of pauli spin blockade: A window into the sources of spin relaxation in silicon quantum dots. *Phys. Rev. B*, 86:115322, (2012).

[36] R. Li, F.E. Hudson, A.S. Dzurak, and A.R. Hamilton. Pauli spin blockade of heavy holes in a silicon double quantum dot. *Nano Lett.*, 15:7314 – 7318, (2015).

[37] H. Bohuslavskyi, D. Kotekar-Patil, R. Maurand, A. Corna, S. Barraud, L. Bourdet, L. Hutin, Y.M. Niquet, X. Jehl, S. De Franceschi, M. Vinet, and M. Sanquer. Pauli blockade in a few-hole PMOS double quantum dot limited by spin-orbit interaction. *ArXiv e-prints:1607.00287*, (2016).

[38] O.N. Jouravlev and Yu.V. Nazarov. Electron transport in a double quantum dot governed by a nuclear magnetic field. *Phys. Rev. Lett.*, 96:176804, (2006).

[39] W.A. Coish and F. Qassemi. Leakage-current line shapes from inelastic cotunneling in the pauli spin blockade regime. *Phys. Rev. B*, 84:245407, (2011).

[40] W.J. Childs and L.S. Goodman. Hyperfine structure of ge^{73} in the $^3p_1$ and $^3p_2$ atomic states and the nuclear magnetic dipole moment of ge^{71}. *Phys. Rev.*, 141:15–21, (1966).

[41] B. Voisin, R. Maurand, S. Barraud, M. Vinet, X. Jehl, M. Sanquer, J. Renard, and S. De Franceschi. Electrical control of g-factor in a few-hole silicon nanowire mosfet. *Nano Lett.*, 16:88 – 92, (2016).